Journal of Power Sources 213 (2012) 186–202

Contents lists available at SciVerse ScienceDirect

Journal of Power Sources

journal homepage: www.elsevier.com/locate/jpowsour

Assessment on hermetic property and mechanical compatibility of various groove-gasket sealing designs for solid oxide fuel cell stack

N. Punbusayakul [a], K. Boonsiri [b], S. Charojrochkul [c], B. Fungtammasan [d], J. Charoensuk [a,*]

[a] Department of Mechanical Engineering, Faculty of Engineering, King Mongkut's Institute of Technology Ladkrabang, Bangkok 10520, Thailand
[b] Department of Mechanical Engineering, Faculty of Engineering, Mahanakorn University of Technology, Thailand
[c] National Metal and Materials Technology Center, Pathumthani 12120, Thailand
[d] King Mongkut's University of Technology Thonburi, Bangkok, Thailand

ARTICLE INFO

Article history:
Received 10 January 2012
Received in revised form
6 April 2012
Accepted 7 April 2012
Available online 19 April 2012

Keywords:
Compressive seal
Gas leakage
Groove
SOFC

ABSTRACT

Assessment among various groove-gasket designs under solid oxide fuel cell operating condition is presented. The gasket is deformable under the stress applied by external loading between 0.13–0.67 MPa. The operating temperature is from 30 to 800 °C. It has an indicated width of 1.95 mm and depth of 2.1 mm., which is accommodated in a square, triangular and U groove channel having the dimension of 2.0 × 2.0 mm^2. From the results, the U shape configuration provides the best performance with immeasurable leak rate under the applying load represented in term of global stress of 0.67 MPa. A stress analysis using Finite Element Method (FEM) tool, ABAQUS™, suggests sufficiently high compressive stress far exceeding the elastic limit with enough coverage of such high-stress area for U-shape design. In contrast, those from square and triangular designs posses relatively lower well-distributed stress and smaller region of highly concentrated stress, respectively. The associated deformed cross section suggests that the gasket has plastically deformed toward the U-shape wall surface at a greater degree than those for triangular-shape design. It can be concluded that the greater region in deformed gasket surface can more effectively reduce interconnectivity of micro channel on the interface between the gasket and the interconnector surfaces.

© 2012 Elsevier B.V. All rights reserved.

1. Introduction

Fuel cell is one of the major areas of current research on alternative energy technology as it uses hydrogen which can potentially come from environmentally friendly energy resource i.e. wind or solar etc. There are various types of fuel cells combining different anode, electrolyte, and cathode materials, i.e.; a solid oxide fuel cell (SOFC) operating at 500–1000 °C [ηth ~45–65%LHV] if combined with a cogeneration system, will provide higher efficiency than the conventional power plants [1–3]. Design factors of SOFC involve fuel processing, power electronics, stack/systems performance & modeling and cell/stack materials & manufacturing. One of major development of the cell/stack materials & manufacturing is on fuel and oxidant seal design to prevent a fuel leakage from the interconnectors to the cells. Failure to meet such requirement drastically reduces the electro-chemical reaction efficiency and lead to a cell damage. Therefore, a prevention of leakage at the interconnector joint is focused in this development, although there are other necessities in property of sealing material, such as; hermetic, coefficient of thermal expansion compatibility, electrical insulating capability, thermal cycle stability, long-term chemical stability with other SOFC components, and deformation characteristic under compressive loading. Never the less, the design must be low in cost and easy to apply with other stack components. Meanwhile, a sealing design could also affect the thermal stress distribution in an SOFC stack during low and high temperature operation.

The sealing development for SOFC can be classified into rigid and compressive seals [4]. Rigid seals require small load when compared with compressive seals during operation and have an excellent hermetic property. The typical of rigid seals are glasses, glass ceramics and brazes sealants. For SOFC application, efforts have been made on modification of the material composition in

* Corresponding author. Tel.: +66 816177658, fax: +66 27392853.
E-mail addresses: kcjarruw@kmitl.ac.th, jarruwat_c@hotmail.com (J. Charoensuk).

0378-7753/$ – see front matter © 2012 Elsevier B.V. All rights reserved.
doi:10.1016/j.jpowsour.2012.04.017

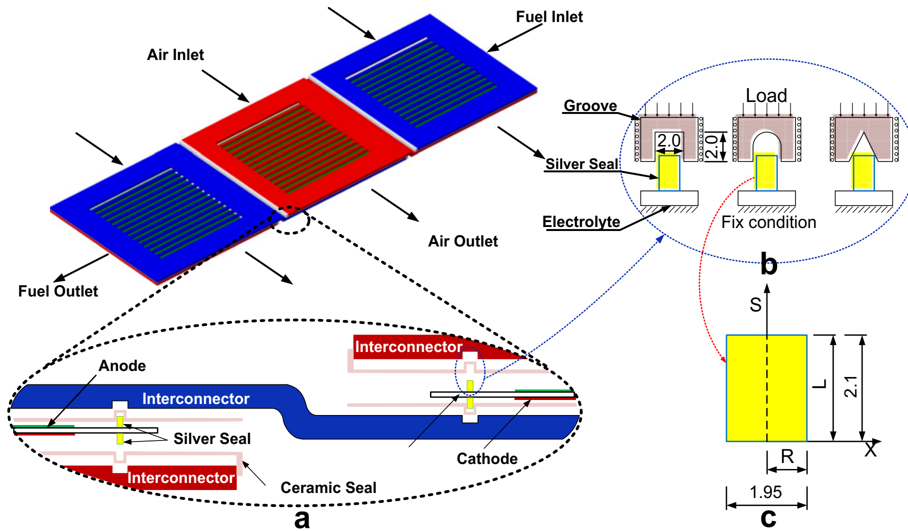

Fig. 1. (a) Schematic diagram of a planar segmented-cell-in-series planar solid oxide fuel cell stack, (b) designs of groove; square, U and triangular shape, and (c) coordinate of pre-deformed silver seal cross section.

order to have compatible thermal expansion coefficient with other cell materials [4–9]. Glass is a versatile material which has been widely used for sealing in the ongoing development of high temperature planar solid oxide fuel cell [9]. Ceramic adhesives and glass composites have been investigated for use as a sealing material for SOFC based on yttria-stabilized zirconia (YSZ) electrolyte and 430 stainless steel interconnector systems in the operating condition of SOFC at 800 °C [10]. The composite seal was designed to be chemically compatible with the ceramic electrolyte (YSZ) and the interconnector (AISI 430, Crofer 22 and FeCr), and suitable thermo-mechanical properties [11–13]. In previous work, this sealing material had achieved a low leakage rate, long-term stability at operating temperature and chemical compatibility with other components. The seal is a composition

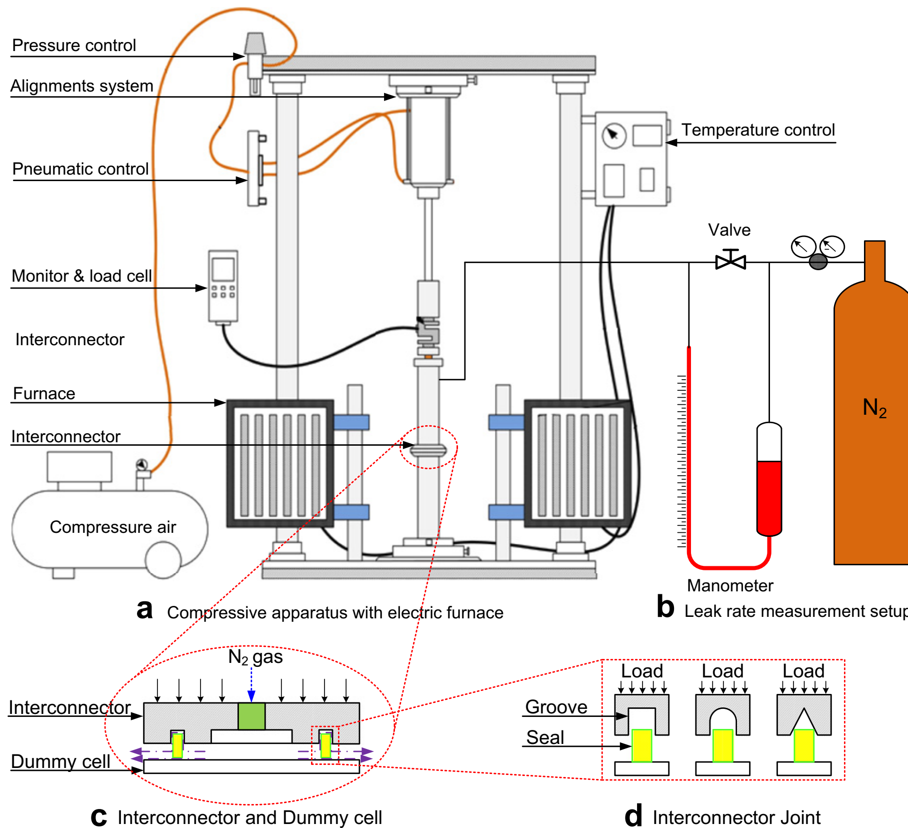

Fig. 2. (a) Compressive apparatus and electric furnace, (b) leak rate measurement setup, (c) interconnector and dummy cell, and (d) interconnector joint.

of polymer blend and glass of ratio 1:3, 1:1 and 3:1 by weight. The effect of glass composition, operating temperature and compressive forces on the leakage rate have been discussed and correlated [9].

Compressive seals require a load application to seal during operation. The most common materials of compressive seals are both non-metallic and metallic [4] i.e. for non-metallic such as mica and ceramic based compressive seals and for metallic such as silver, gold and platinum. For both types of compressive seal, the structure is like a layer of sandwiches of hybrid material [14–16]. Therefore, the thermal expansion mismatch of compressive seals is not as severe as that of rigid seals during thermal cycling, because the compressive sealant is non-bonded [14–23]. However, the use of compressive seals could generate certain stresses in components. Thus, the thermo-mechanical behavior of components assembled as compressive seal and their associated stress distribution in SOFCs operating environment should be evaluated. Some researchers [3,14–28] used experimental and/or numerical methods to study the mica based, metal-foil based, bonded compliant seal (BCS), compressive seal adjacent metallic or ceramic interconnects and positive electrode–electrolyte–negative electrode (PEN) in multi-cell pSOFC stacks. Comprehensive thermal stress was analyzed by using a FEA model in such a compliant sealing design [26]. The results showed that the bending deformation in PEN leading to a well joined structure, and the critical stress in PEN was low at room temperature but increased with temperature up to the operating condition due to change in sealing design [20]. It was found also that the glass-ceramic seal induced the highest stress concentration in the PEN whereas the BCS induced relatively low stresses in the PEN [21]. From research on leak rate behaviors of mica material [17,18], the leak rate decreased more than 60% at 800 °C after 18 thermal cycles. Our previous investigation on the effect of load patterns applying on the interconnector based on loading conditions, surface roughness and the width at the interconnector joint on sealing performance. Silver and Termiculite 866 materials were used to determine these parameters influence on the leakage rate [29,30]. At the same time, our research counterpart [31] had designed a cell stack in which the cell is separated from one another and each cell is connected in series as shown in Fig. 1 (a). With this stack configuration, the metal seal material with high flexibility can be applied to prevent leakage of SOFC. Moreover, due to a small initial gauge length of each cell unit that creates a small elongation of the interconnector at high temperature, the induced stress created by this mismatch of thermal expansion coefficients between cell and interconnector can be minimized. The material with high flexibility such as platinum and gold are able to perform under high temperature as well but platinum and gold are more expensive than silver.

1.1. Objective of this research

This paper presents the achievement made from the design of the groove to prevent leakage of hydrogen in the cell stack. The design is based on a compressive load (global stress of 0.13–0.67 MPa) at 30–800 °C and for the design of groove of square, U and triangle cross sections, having the width of 2 mm and depth of 2 mm. The seal material is silver (99.99 wt%) as shown in Fig. 2. The force distribution on seal material is presented by Finite Element Method (FEM) and the leak rate is measured using a manometer (ASTM F 37–89). It is also worth noting here that the term "global" stress is defined as the applied load per unit projected area of the seal.

2. Experiment setup

2.1. Material property

To make an effective use of a finite element method for assessment of thermal stress distribution, it would be better to use a simulation model as close as possible to the practical applications [32,33]. All of the test specimens (silver 99.99 wt%, 10 specimens per temperature) are fabricated from the same batch of material. The material properties, i.e; proportional limit (P), strength (Y), ultimate strength (U), fracture point, elongation percentage, modulus of elasticity, melting point and their effects due to temperature change have been obtained experimentally at 30, 100 and 200 °C using a universal testing machine (UTM). The experimental data are analyzed to show the effect of temperature on

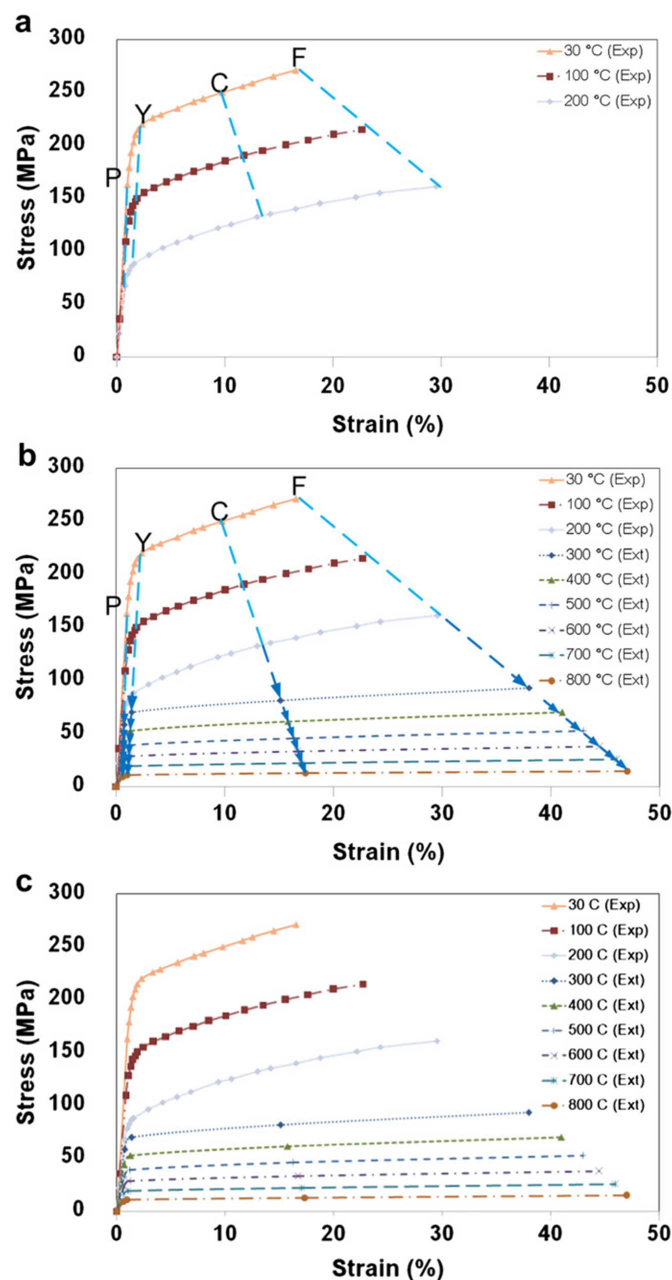

Fig. 3. The stress–strain relationship of silver at various temperatures (30–200 °C) from experimented results and from extrapolation from 300 to 800 °C.

those parameters for elastic and plastic modes. The interpolation for values from 200 upto 800 °C has been made to obtain a mechanical behavior of silver material by knowing the fact that all mechanical properties will be those of liquid form of silver at melting temperature (961 °C). Therefore, the predicted values of mechanical properties between 200 °C up to the values prior to the melting temperature can be obtained by the numerical interpolation functions. see Section 3.1.

2.2. Problem specification for finite element analysis

Commercial FEA code was used to calculate the thermal stress distributions in an interconnector joint of a planar SOFC. Depicted in Fig. 1 (b) are cross sections of square, U and triangular grooves. The coordinate of silver seal cross section is shown in Fig. 1 (c). Only the individual component with line contact is considered to reduce the computation time. It is assumed in this study that the type of contact between components such as; silver seal, single cell and interconnector components are frictionless. Stresses by self-weight of components are small compared to external load such that they are neglected in this simulation. The simulation is based on dynamic, explicit and direct method. It is also assumed that the SOFC components are isotropic and homogeneous. Deformation of silver seal is assumed plastic, but; a metallic-ceramic interconnector and a cell are assumed elastic since the ultimate stress values of these materials are higher than that of silver seal. The seal model consists of a silver seal, metallic-ceramic interconnector and the cell. Moreover, the elastic modulus of interconnector at room temperature is 200 GPa. Since the size of the interconnector is large compared to the size of the seal and the deformed surface is relatively small, the value is assumed constant throughout the temperature range up to 800 °C. Poisson's ratios of 0.17 and 0.37 and thermal expansion coefficients of 17.3E-6 and 18.9E-6 are used for metallic-ceramic and silver at all given temperatures. The sizes of silver seal and groove are 1.95 × 2.1 mm^2 and 2 × 2 mm^2, respectively. As for an element type, a 4-node bilinear plane stress quadrilateral, reduced integration (CPS4R) is employed.

2.3. Profile test

This section describes the material characteristic for use in a simulation model and to validate the deformation of the simulation result. A sample preparation of silver seal material was carried out using a size of 2 × 2.1 mm^2 from the gap between an interconnector and a dummy cell as shown in Fig. 2 (c) and (d). The complete device was located in a furnace and loaded by a compressive apparatus at 0.67 MPa. The samples are subjected to increasing temperature from ambient condition to 800 °C at the heating rate of 1 °C min^{-1}. After maintaining at the specified temperature for 2 h, the samples are cooled down at the rate of 1 °C min^{-1}. Then, the deformed seal was taken out, cut and polished for prior to performing a microstructure analysis.

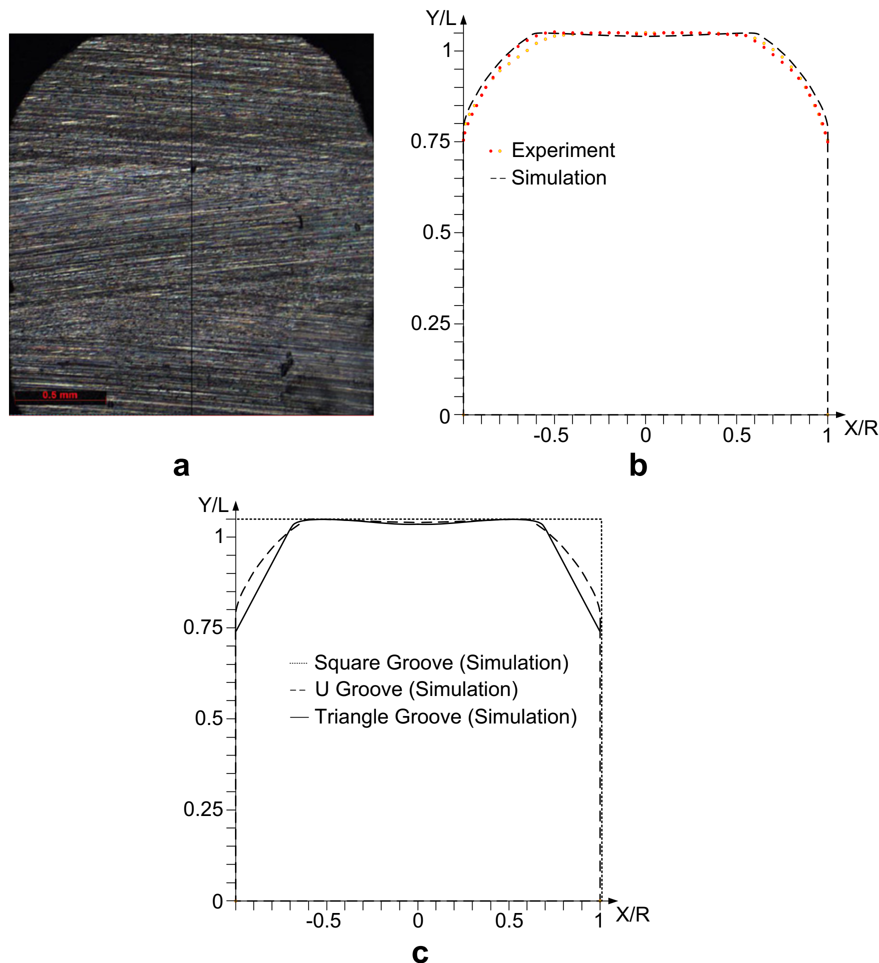

Fig. 4. (a) Profile curve of silver seal at 800 °C and 0.67 MPa using an optical microscope, (b) a comparison of profile curve for silver seal at 800 °C and (c) a comparison between simulated profile curves of square, U and triangular groove at 800 °C and 0.67 MPa.

2.4. Compressive apparatus with electric furnace and leak rate measurement setup

A vertical electric furnace is designed to accommodate a fuel cell stack. An inconel tube is supported by an alignment system to generate a compressive force to the interconnector surface as shown in Fig. 2 (a). The leak rate measurement setup was constructed according to ASTM F 37–89 as shown in Fig. 2 (b). The measurements of leak rate are carried out at 30 °C, and at the temperature of 400–800 °C. The heating rate is 1 °C min^{-1}. After

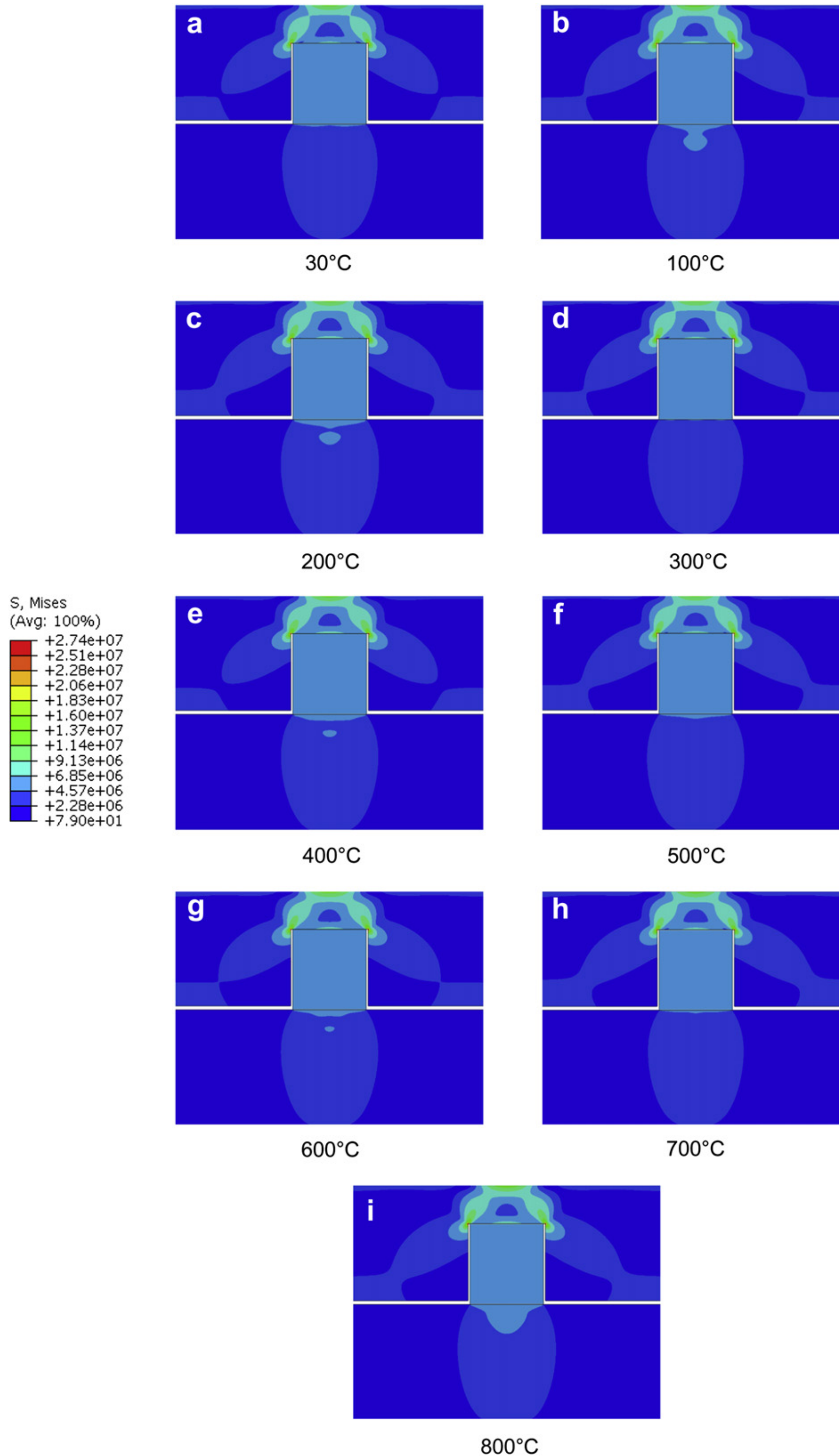

Fig. 5. Simulated stress distribution on rectangular silver seal, groove and dummy materials at various temperatures, (a) 30 °C, (b) 100 °C, (c) 200 °C, (d) 300 °C, (e) 400 °C, (f) 500 °C, (g) 600 °C, (h) 700 °C, and (i) 800 °C.

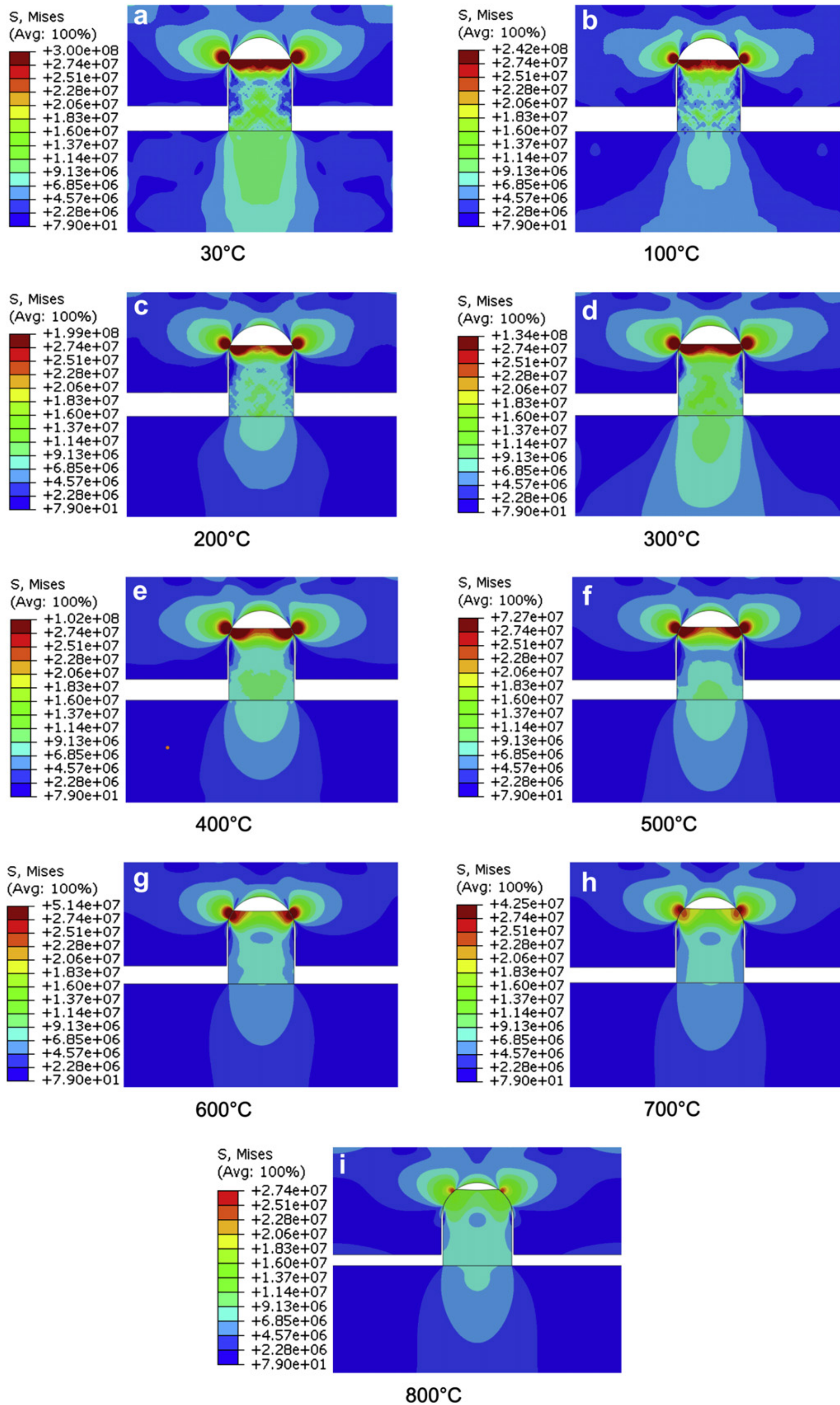

Fig. 6. Simulation of stress distribution on cross section of silver seal in a U groove at various temperatures, (a) 30 °C, (b) 100 °C, (c) 200 °C, (d) 300 °C, (e) 400 °C, (f) 500 °C, (g) 600 °C, (h) 700 °C, and (i) 800 °C.

the temperature level is kept constant for 30 min, the amount of leak gas is measured for 30 min. The pipeline is filled with N_2 at 2 bar gauge. When the valve is turned off, the gas passes into the manometer and replaces the liquid inside the U tube for a measurement of leakage. The cooling down rate of 1 °C min^{-1} was chosen as the best experimental condition in terms of interface morphology. Circular seals with an outer diameter of 50 mm and 46 mm inner diameter are tested. Samples are placed in between two faces of a 316 stainless steel mold. This assembly is used to simulate the sealing condition with a metallic interconnector. The complete device is located in a furnace and loaded by a compressive apparatus. All experiments are conducted under applying load of 0.13–0.67 MPa. The test arrangement is shown in Fig. 2 (c) and (d).

3. Result and discussion

3.1. Material properties

As the operating temperature for the given SOFC is around 800 °C, material properties at such a high temperature are required to obtain more reliable simulation results. The material properties, i.e.; Proportional limit, Strength, Ultimate strength, Fracture point, Elongation limit, Modulus of elasticity and melting point and their effects due to temperature change are obtained experimentally for 30, 100 and 200 °C [32,33]. In our investigation, the test data are obtained from tensile tests over the same range of temperatures using wire-type specimens as shown in Fig. 3a. The predicted data at temperature range of 300–800 °C are obtained using our validated interpolation method, see Fig. 3b. The detail of this method will be discussed elsewhere [34], considering the material's properties are temperature dependent on elastic and plastic modes. For the metallic and ceramic materials, they are assumed to deform elastically up to the yield limits at both room temperature and operating temperature. The data at elevated temperatures show distinct softening effect on the strength of the materials. The obtained stress–strain curves of silver material at different temperatures reveal that the tensile strength and elastic modulus decreases with increasing temperature. The complete true stress–strain curve data are imported into FEA calculation.

3.2. Profile curve of silver material versus simulation

In Fig. 4 (a), the dimensional result is used for validation with the simulation result of profile curve for U groove design. Small discrepancies i.e.; under-predicted (1.5–3%), at $X/R = 0$ and $S/L = 1$ and over-predicted (1–5%, $X/R = 0.6$–1, $S/L = 0.75$–1) values are shown in Fig. 4 (b). Considering large deformation of material, this is a sufficient method for obtaining the material property of silver at high temperature. By using this validated method on square and triangular grooves, the profile curves of seal subjected to the same operating condition, 800 °C and 0.67 MPa, are given in Fig. 4 (c). The results under U groove design agree well with the experiment. As for triangular groove, additional investigation is carried out and it is found that the profile is inconsistent as it varies significantly among different sampling's locations. This is due to large deformation and interfacial slip taking place in relatively larger region during compression at high temperature leading to greater uncertainty of experimental result. Nevertheless, general conclusion can be made such that the greatest contact interface is from square groove where the less are those from U and triangular groove, respectively.

3.3. Effect of temperature on stress distribution at the material seal cross section

In the following subsections, numerical simulation for each component of square, U and triangular grooves is presented individually. In current study, the effect of temperature on stress distribution on the interconnector joint is investigated. The calculated stress distribution is based on the design of groove; i.e. square, U and triangle (shown in Fig. 1 (b)). The applying load of 0.67 MPa at different temperatures (30 °C, 100–800 °C) is used. The material properties and problem specification for finite element analysis has already been mentioned in Sections 2.1 and 2.2 respectively.

3.3.1. Square groove

The calculated stress fields on each component of the interconnector joint based on square groove under compressive load of 0.67 MPa at various temperatures are illustrated in Fig. 5. The coordinate of groove, silver seal and single cell cross section are given in Fig. 1 (b) and (c). The concentration of stress is represented by a relatively small zone of red color. The critical stress is found at corner locations $S/L = 1$, $X/R = -1$ and 1 of square groove, and their values are higher than 27.4 MPa. However, the stress on silver seal is significantly lower which is about 5.17 MPa. Similarly, the stress distributions at the contact surface between components, which are; i) between the groove and silver seal at the top location ($S/L = 1$, $-1 < X/R < 1$) and between silver seal and dummy cell at the bottom location ($S/L = 0$, $-1 < X/R < 1$) are almost uniform (~5.17 MPa). Moreover, the maximum Von Mises stress does not significantly change with temperature. Lastly, the contact surface of silver seal in the square groove at the top and bottom location ($S/L = 0$ and 1, $-1 < X/R < 1$) does not significantly increase nor decrease (~2 mm) with the increased temperature.

3.3.2. U groove

Cross sectional distributions of Von Mises stress on components of interconnector joint based on U groove design with an applied global compressive stress of 0.67 MPa (average stress calculated from applying load divided by projected area of seal in the interconnector) at various temperatures are presented in Fig. 6. The results show that the maximum stress of U groove is at contacting surface at the top location between the groove and silver seal. Table 1 is the maximum stresses of U groove at the top location between the groove and silver seal at the corresponding temperatures.

As far as the top surface of the seal component is concerned, the stress of silver seal is the highest at the top corner locations as the material is deformed under containment of groove channel. The stress field on seal cross section, although not evenly distributed, is getting more uniform when the operating temperature increases. As mentioned earlier for 30 °C the maximum stress in that region is as high as 300 MPa while reducing to 31.6 MPa at the center location ($S/L = 1$, $X/R = 0$). The difference between the values on these locations at the SOFC operating temperature (800 °C) of both regions are much closer to each other, yielding the maximum and minimum of 16.2 and 11.6 MPa, respectively.

Similarly, stress concentration is found at the contact between silver seal and dummy cell near the center of the bottom location ($S/L = 0$, $X/R = 0$). Consider at 30 °C the maximum stress is around 16.2 MPa, while the stress at side location of the bottom plane

Table 1
The maximum stress of U groove is at contacting surface at the top location between the groove and silver seal.

Temperature (°C)	30	100	200	300	400	500	600	700	800
Maximum stress (MPa)	300	242	199	134	102	72.7	54.1	42.5	14.7

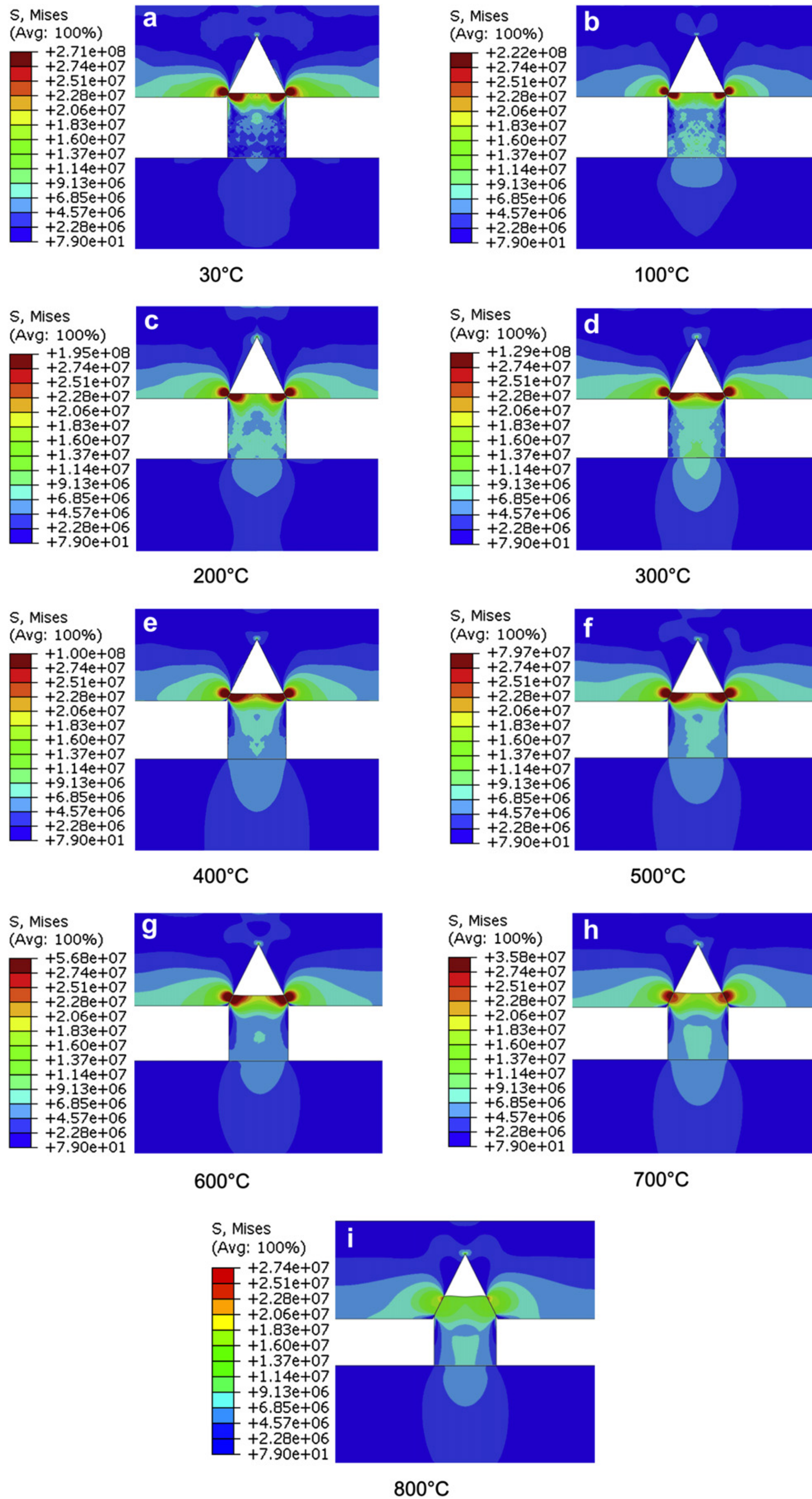

Fig. 7. Simulation stress distribution on cross sections of silver seal in a triangular groove at various temperatures, (a) 30 °C, (b) 100 °C, (c) 200 °C, (d) 300 °C, (e) 400 °C, (f) 500 °C, (g) 600 °C, (h) 700 °C, and (i) 800 °C.

(S/L = 0, X/R = −1 and 1) is slightly lower with the value of 13.8 MPa. With softening effect due to an increase in temperature, for instance upto 800 °C, the maximum stress at the center of the bottom of silver seal is found at about 8.3 MPa and the maximum stress at the side location of the bottom plane is a little bit greater than 6.8 MPa. The maximum stress obviously decreased with increasing temperature.

An essential feature which requires attention is that the contact surface of silver seal in U groove at the top location (S/L = 1, −1 < X/R < 1) rapidly increases with increasing temperature. While global compression loading is effectively equal but the strength of silver decreases with temperature, the silver seal deforms at greater degree in response to increasing in temperature. This is due to softening effects that enhance the plastic deformation of seal material. Meanwhile, the contact surface at the bottom location (S/L = 0, −1 < X/R < 1) is irresponsive to change in temperature.

3.3.3. Triangular groove

The distribution of stress on cross section of triangular groove with an applied compressive stress of 0.67 MPa (average stress calculated from applying load divided by its perpendicular area) at various temperature are depicted as Fig. 7. As a result, the most critical stress of triangular groove is on contacting surface between the groove and silver seal at the top location in Table 2 when the temperature increases from 30 °C to 800 °C.

Generally, the Von Mises stress of silver seal is highest at the top corner location. At 30 °C the critical stress is higher than 261 MPa, while the stress at center of the top location (S/L = 1, X/R = 0) is approximately at a value of 23.9 MPa. However, the maximum and minimum stresses at operating temperature (800 °C) of both regions are 14.7 and 13.1 MPa respectively.

As far as the corresponding Von Mises stress of a dummy cell is concerned, the maximum value is found near the center of the bottom location (S/L = 0, X/R = 0) at around 12.2 MPa, but slightly decrease along the distance from the center of bottom location to 9.0 MPa. As the temperature changes from 30 °C to the operating temperature, the maximum stress at the center of the bottom location changes from 12.2 MPa to 7.7 MPa. Moreover, the stress at the left and right corners of the bottom location changes from 9.0 MPa to 4.4 MPa. These indicate that the stress intensity decreased significantly with temperature. In other words, thermal effect on material property must be considered for determination the distribution of stress on each component.

It is important to note here that the contact surface between silver seal with triangular groove at the top location (S/L = 1, −1 < X/R < 1) has slightly increased with increasing in temperature. Softening effect due to increase in temperature is responsible for this observation, see also the change in mechanical property of silver with temperature in Fig. 3. However, the contact surface at the bottom location (S/L = 0, −1 < X/R < 1) remain constant for all temperature range of this study.

3.4. Effect of groove design on stress distribution between square, U and triangular groove at 800 °C

To illustrate the effect of groove design on stress distribution upon each member of the interconnector joint among square, U and triangular grooves, the contour plots with identical legend color are presented in Fig. 8. All cases are performed under identical external compressive load (0.67 MPa, global stress) material type, dimension (width and height) and operated at temperature of 800 °C, which may be seen in Fig. 1 (b), Fig. 1 (c), Section 2.1 and 2.2, respectively.

The maximum stress of square groove is found at the corner of the groove at locations S/L = 1, X/R = −1 and 1, but the maximum stress of U and triangular grooves are highest at the top corner location and their values are around 27.4 MPa.

Generally, the stress of silver seal cross section for square groove is almost uniform at about 5.17 MPa at the top location

Table 2
The most critical stress of triangular groove is on contacting surface between the groove and silver seal at the top location.

Temperature (°C)	30	100	200	300	400	500	600	700	800
Maximum stress (MPa)	271	222	195	129	100	79.7	56.8	35.8	14.7

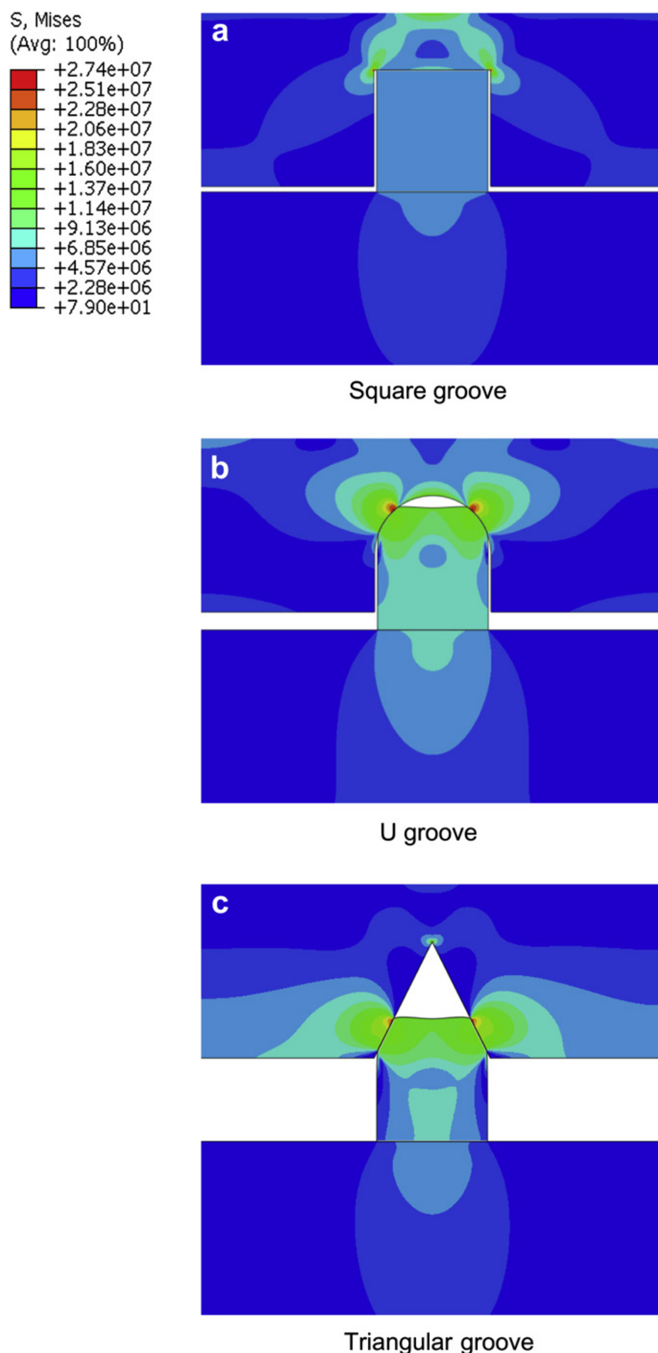

Fig. 8. Simulation of stress distribution on cross section of silver seal for various grooves at 800 °C, (a) square groove, b) U groove, and c) triangular groove.

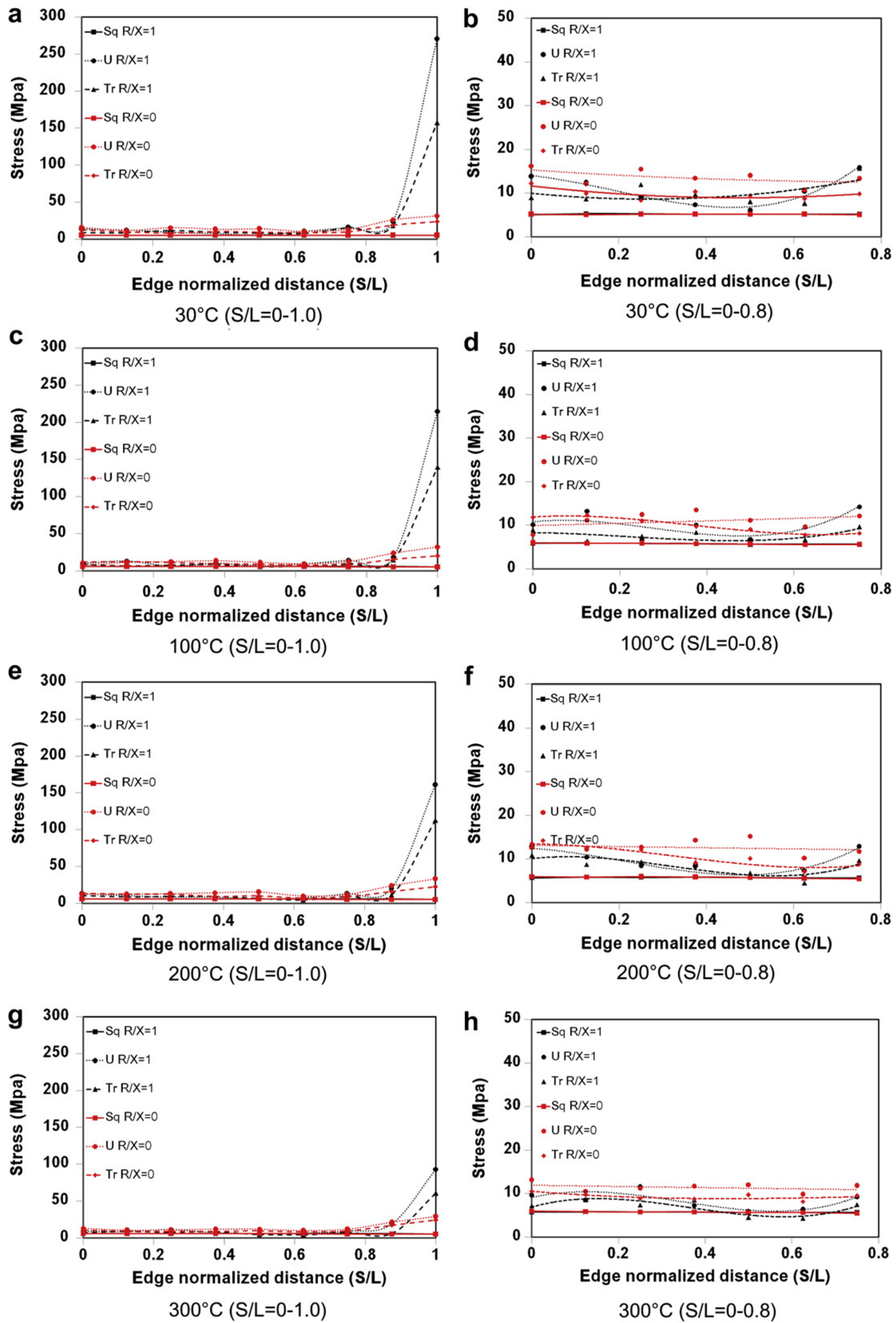

Fig. 9. Stress on the cross section of silver seal under the square, U and triangular grooves confinement; (a) 30 °C (S/L = 0–1.0), (b) 30 °C (S/L = 0–0.8), (c) 100 °C (S/L = 0–1.0), (d) 100 °C (S/L = 0–0.8), (e) 200 °C(S/L = 0–1.0), (f) 200 °C(S/L = 0–0.8), (g) 300 °C (S/ = 0–1.0), (h) 300 °C (S/L = 0–0.8), (i) 400 °C (S/L = 0–1.0), (j) 400 °C (S/L = 0–0.8), (k) 500 °C (S/L = 0–1.0), (l) 500 °C (S/L = 0–0.8), (m) 600 °C(S/L = 0–1.0), (n) 600 °C(S/L = = 0–0.8), (o) 700 °C(S/L = 0–1.0), (p) 700 °C(S/L = 0–0.8), (q) 800 °C(S/L = 0–1.0) and (r) 800 °C(S/L = 0–0.8).

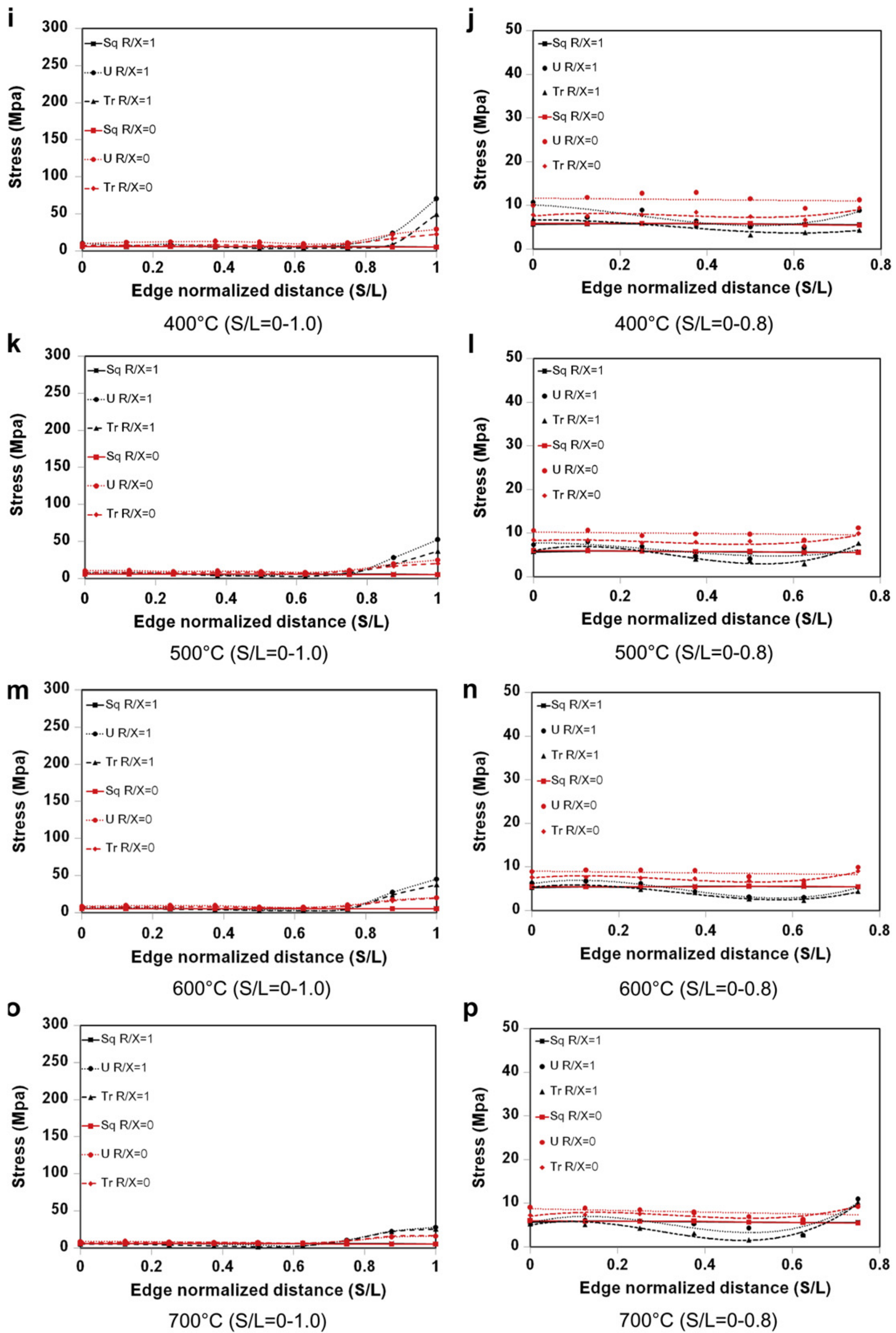

Fig. 9. (*continued*).

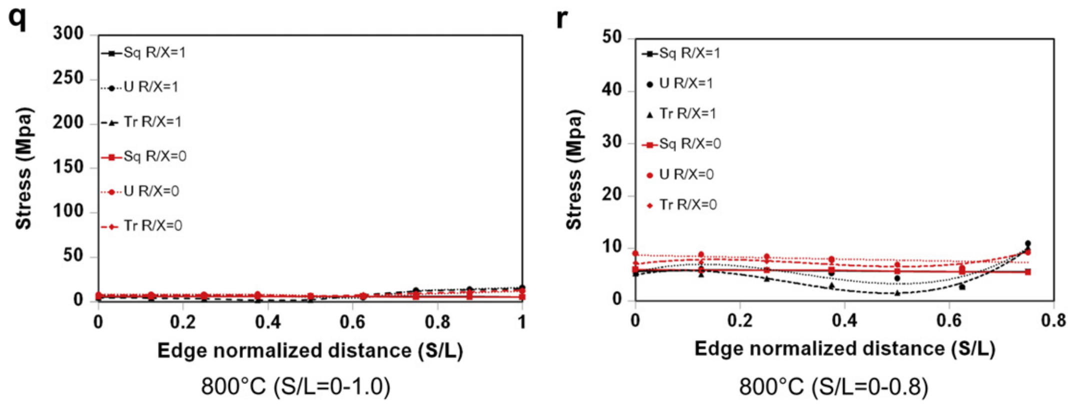

Fig. 9. (*continued*).

(S/L = 1, −1 < X/R < 1), but the maximum stress of silver seal for U and triangular grooves are highest at the top corner locations and their values are around 18 and 14.7 MPa, respectively. These maximum stresses of seal under U and triangular grooves are enhanced by 217% and 188% compared with that under the square groove. Additionally, it also leads to the difference in stress distribution of silver seal at the bottom location (S/L = 0, −1 < X/R < 1). The stress for U and triangular grooves is relatively high near the center of the bottom location (S/L = 0, X/R = 0) and the value is around 8.3 and 7.7 MPa respectively, which is 79% and 50% higher than the base case. The corresponding stress value at far end of the bottom location of silver seal is approximately at 6.8 and 4.4 MPa which is 33% greater and 13% less than the value of the base case, respectively.

As far as the contact surface between a silver seal and a square groove is concerned, the area of contact at the top (S/L = 1, −1 < X/R < 1) does not change with temperature (approx. 1.95 mm width). Meanwhile, the contact surface of silver seal inside U and

Table 3
The maximum stresses is observed on the top location around the contact point (S/L = 1 and R/X = 1).

Temperature (°C)		30	100	200	300	400	500	600	700	800
Maximum stress (MPa)	U groove	271	215	161	93.2	70.2	52.3	45.3	28.0	16.2
	Triangular groove	157	139	112	60.6	49.1	37.7	36.6	25.4	14.7

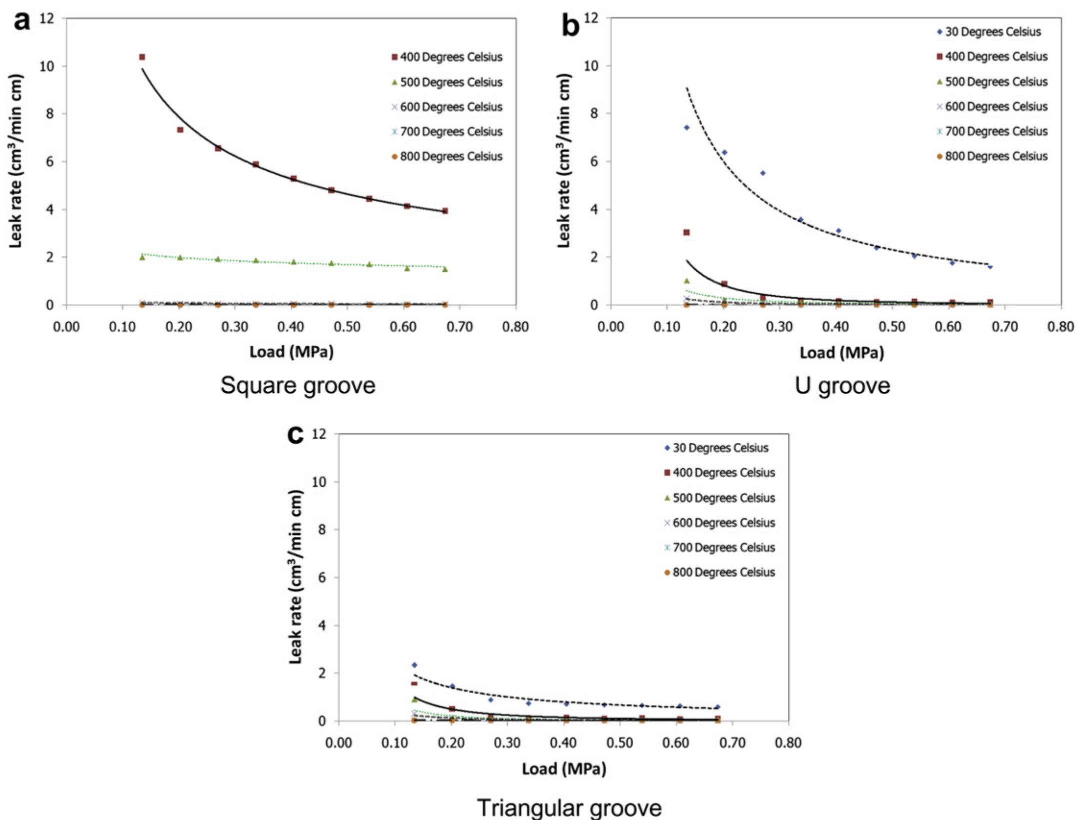

Fig. 10. Relationship of leak rate with loading at various temperatures, (a) square groove, (b) U groove, and (c) triangular groove.

triangular groove at the top location (S/L = 1, −1 < X/R < 1) is reduced by 27.7% and 37.7% respectively. However, the contact surface of silver seal at the bottom location (S/L = 0 and 1, −1 < X/R < 1) remains the same for all types of groove.

3.5. Dispersion of stress on cross section of silver seal under constrains of various groove designs

In this section, the dispersion nature of stress on silver seal between square (Sq), U and triangular (Tr) groove is presented. Illustrated in Fig. 9 are results of numerical simulation trials under overall compressive stress of 0.67 MPa at temperature range of 30 °C–800 °C. The profiles of stress along the deformed edge, corresponding to R/X = 1, and along the less-deformed middle plane, R/X = 0 are given. Ones should note here that the distance along the deformed edge does not always refer to the vertical distance. This is due to displacement occurred under constrains of the groove channel. Transformation from intense stress in region near the contact surface to relatively less stress intensity inside the seal material is observed. It suggests a transfer of compressive force from contact surface at the top location of silver seal to its bottom location. This is normal characteristic under mechanical contact. The maximum stresses is observed on the top location around the contact point (S/L = 1 and R/X = 1) for U and triangular groove design. The maximum stress values at the corresponding temperatures of 30–800 °C are listed in Table 3.

The dispersion of stress is discussed under two distinctive operating conditions; i.e. at room temperature and at operating temperature as follow.

Firstly, at 30 °C, the stress profile has rapidly decreased with distance from the contact point, S/L = 1 to 0.8 at R/X = 1 from $271_{max,U,R/X=1}$ to $10.7_{avg,U,R/X=1}$ MPa for U groove and $157_{max,Tr,R/X=1}$ to $9.8_{avg,Tr,R/X=1}$ MPa for triangular groove. In contrast, for the profile at R/X = 0, the value slightly decreases

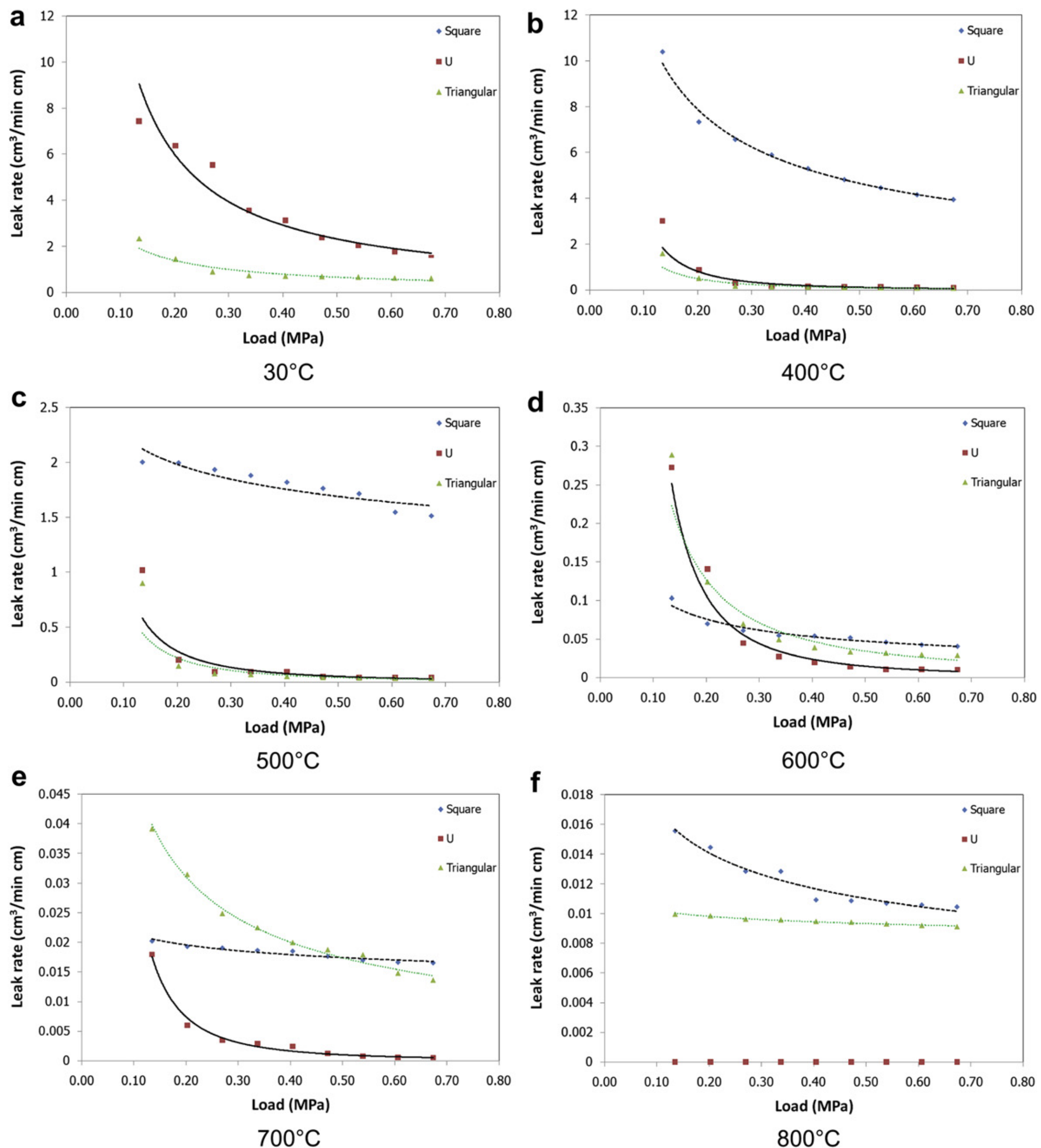

Fig. 11. Relationship of leak rate to compressive loading at 30–800 °C for different groove designs, (a) 30 °C, (b) 400 °C, (c) 500 °C, (d) 600 °C, (e) 700 °C, and (f) 800 °C.

with distance from S/L = 1 to 0.8. The corresponding maximum stress for U groove has decreased from $31.5_{max,U,R/X=0}$ to approximately $13.6_{avg,U,R/X=0}$ MPa, whereas for triangular groove, the maximum stress has decreased from $23.1_{max,Tr,R/X=0}$ to approximately $10.1_{avg,Tr,R/X=0}$ MPa. However, the stress value is almost uniform for square groove. The average stress along the distance from S/L = 0 to 1 at R/X = 1 and 0 is 5.2 and 5.1 MPa, respectively. As far as the stress near the contact point between dummy cell and sealing material is concerned, the value is as low as 5.1–5.2 MPa for square groove. As for U and triangular grooves, however, the value is slightly higher and relatively less uniform. The average stress along the distance from S/L = 0 to 0.8 at R/X = 1 and 0 is $10.7_{U,R/X=1}$, $13.6_{U,R/X=0}$ MPa, for U groove and $9.8_{Tr,R/X=1}$ and $10.1_{Tr,R/X=0}$ MPa for triangular groove, respectively.

Secondly, at operating condition, the stress profile slightly decrease with distance from S/L = 1 to 0.8 at R/X = 1 from $16.2_{max,U,R/X=1}$ to $7.0_{avg,U,R/X=1}$ MPa for U groove and $14.7_{max,Tr,R/X=1}$

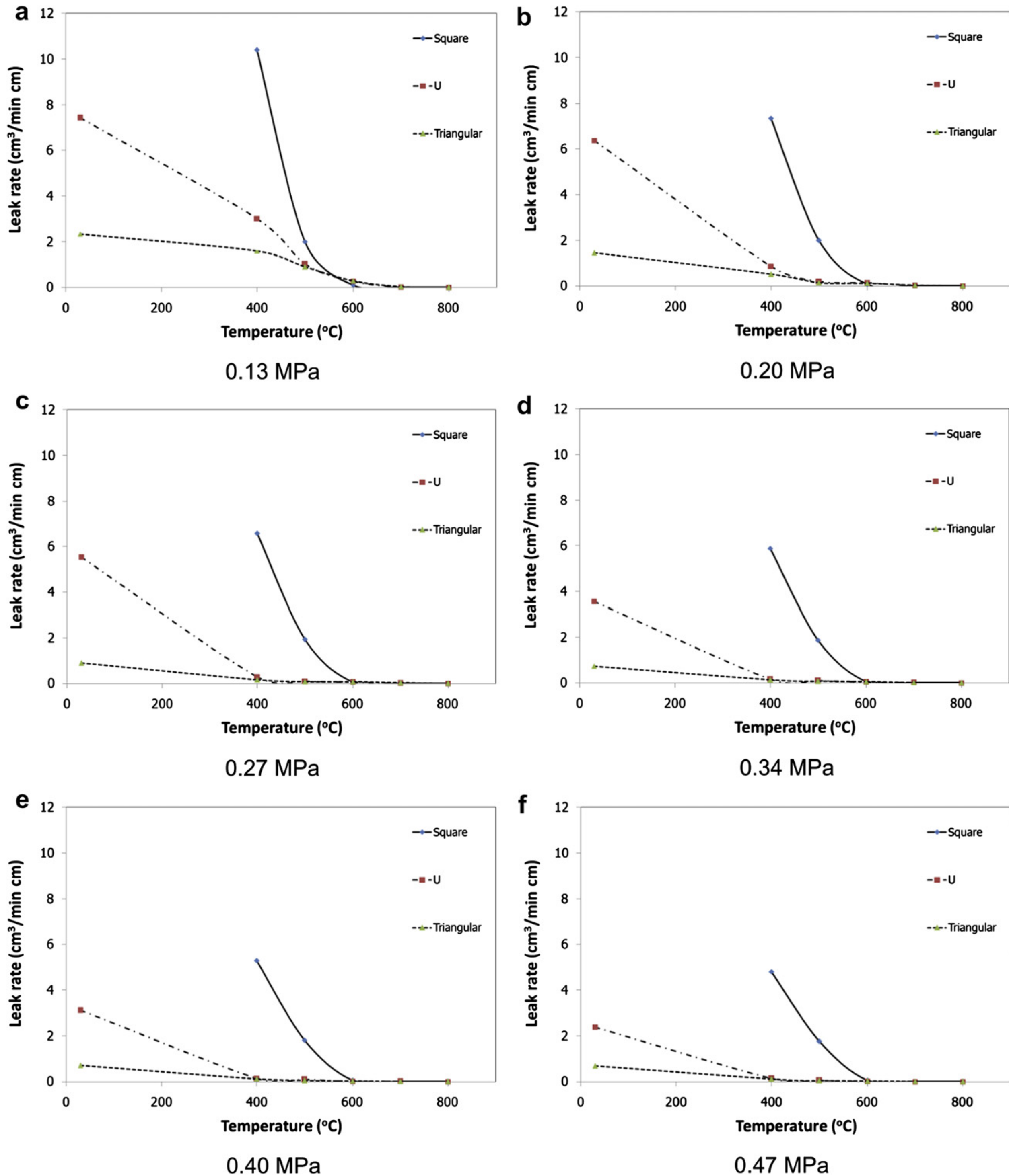

Fig. 12. Relationship of leak rate to temperature and groove design under (a) 0.13 MPa, (b) 0.20 MPa, (c) 0.27 MPa, (d) 0.34 MPa, (e) 0.40 MPa, (f) 0.47 MPa, (g) 0.45 MPa, (h) 0.61 MPa, and (i) 0.67 MPa.

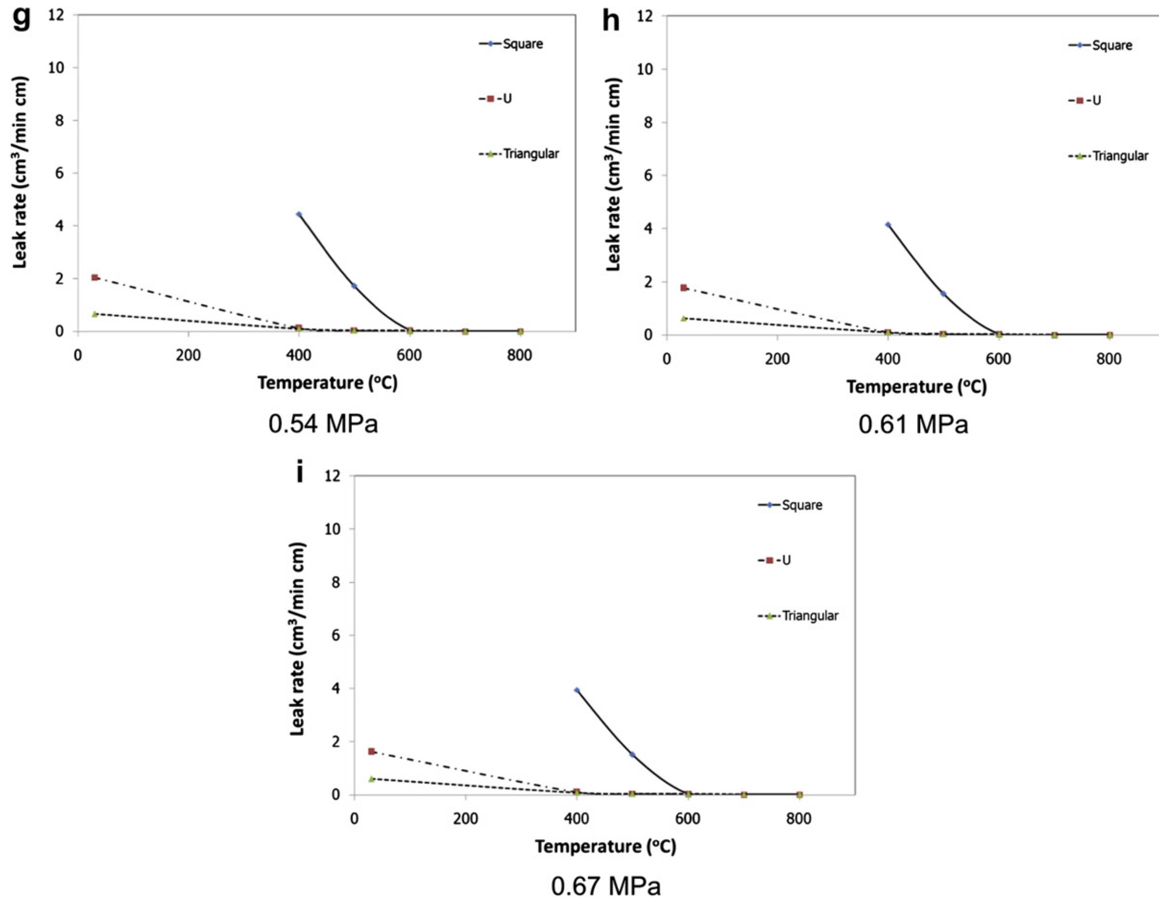

Fig. 12. (*continued*).

to $5.1_{avg,Tr,R/X=1}$ MPa for triangular groove. This observation is in contrast with that operated under room temperature as a result of temperature softening. As for R/X = 0, the profile has slightly decreased with distance from S/L = 1 to 0.8. The value of maximum stress for U groove decreases from $11.6_{max,U,R/X=0}$ at contact point to approximately at $7.7_{avg,U,R/X=0}$ MPa. For triangular groove, the maximum value is $13.1_{max,Tr,R/X=0}$ and decreases to approximately $7.8_{avg,Tr,R/X=0}$ MPa. For square groove, the stress value is almost uniform; i.e. along the distance from S/L = 0 to 1, at R/X = 1 and 0, the value is 5.6 and 5.7 MPa, respectively. As for the stress near the contact point between dummy cell and sealing material, particularly for U and triangular grooves, the value is relatively less uniform than that from the square groove. The average stress along the distance from S/L = 0 to 0.8 at R/X = 1 and 0 is $7.0_{U,R/X=1}$, $7.7_{U,R/X=0}$ MPa, for U groove and $5.1_{Tr,R/X=1}$ and $7.8_{Tr,R/X=0}$ MPa for triangular groove, respectively.

In summary, at 30 °C, U and triangular grooves yield higher average stress at S/L = 0–0.8 and R/X = 0, 1 than that from square groove which is 2.3 and 1.9 times greater, respectively. Similarly, at operating condition, U and triangular groove yield higher average stress at S/L = 0–0.8 and R/X = 0, 1 which is 1.4 and 1.2 times greater, respectively. U groove design is more robust than square and triangular groove designs as it can maintain sufficiently high contact stress over entire temperature range under this investigation.

3.6. Relationship between leak rate, temperature and groove designs

The leak rate was measured from 30 to 800 °C for various groove configurations under loading condition from 0.13 to 0.67 MPa. For square groove design, the highest measurable leak rate is shown in Fig. 10, which is 10.39 cm^3 $(min\ cm)^{-1}$ at 400 °C. For U groove design, the leak rate varies from 7.42 to 0 cm^3 $(min\ cm)^{-1}$, corresponding to operating temperature of 30–800 °C, respectively. Triangular groove provides the lowest leak rate in general at 1.596–0.009 cm^3 $(min\ cm)^{-1}$ (corresponding to 30–800 °C). The leak rate decreases with increasing pressure and temperature.

The leak rate for a square groove at room temperature is as high as 10 cm^3 $(min\ cm)^{-1}$ as shown in Fig. 11. It decreases rapidly at temperature from 400 °C. Above 400 °C, the rate is rather constant despite variation of applying load from 0.1 to 0.7 MPa. However, it varies from 2 cm^3 $(min\ cm)^{-1}$ at 500 °C, 0.3 cm^3 $(min\ cm)^{-1}$ at 600 °C, 0.04 cm^3 $(min\ cm)^{-1}$ at 700 °C, and 0.016 cm^3 $(min\ cm)^{-1}$ at 800 °C. U groove design yields higher leak rate than other designs only at 30 °C. The triangular groove gives higher amount of leak rate than other designs only at 700 °C and under applying pressure up to 0.5 MPa. At 400 and 800 °C however, the leak rate of this design slightly increases with increasing compressive force. The highest leak rate from triangular groove is 2.338 cm^3 $(min\ cm)^{-1}$ (0.13 MPa, 30 °C) and the lowest leak rate is 0.009 cm^3 $(min\ cm)^{-1}$ (0.67 MPa, 800 °C). In general, the square groove gives highest leak rate when compared with other designs. The superiority in hermetic property of U groove design over other designs has become obvious at temperature above 700 °C, see Fig. 11 (i) and (j).

Fig. 12(a–i) shows the leak rate at 30, 400, 500, 600, 700 and 800 °C under particular loading condition from 0.13 to 0.67 MPa. It is obvious that the critical temperature for sealing effect of silver material is 600 °C for all loading conditions and groove designs. This experimental finding is worthwhile for ones looking for a recommended operating condition of silver seal in the SOFC stack.

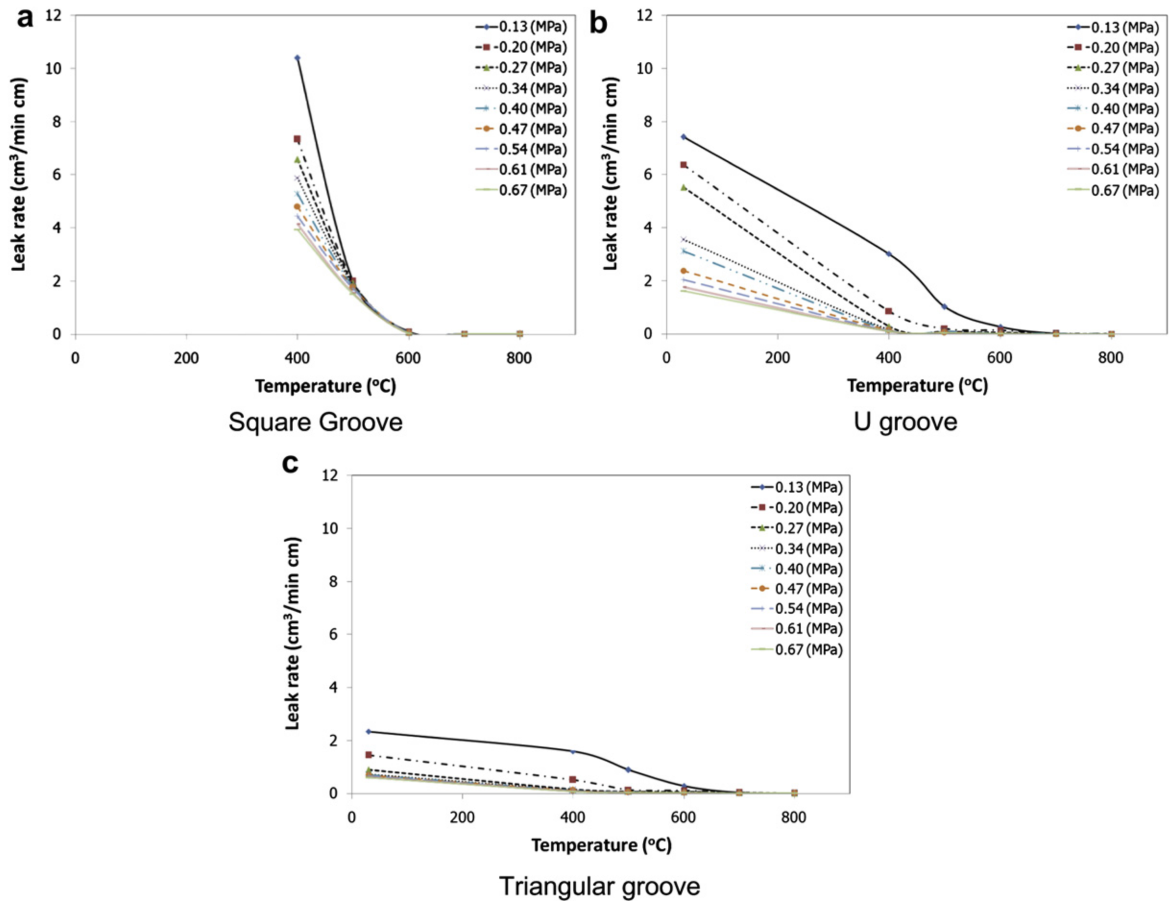

Fig. 13. Variation of leak rate at various temperatures and loading, (a) square groove, (b) U groove, and (c) triangular groove.

From Fig. 13(a–c), hermetic property of square groove is most affected by temperature change as compared with other designs. However, the leak rate for the temperature above 600 °C is higher than those obtained from U and triangular grooves. When consider this with the stress field obtained under different groove designs, it is reasonable to correlate the leak rate with i) the magnitude of desirable stress ii) the mechanical properties of material at corresponding temperature and iii) the coverage of this sufficient high-stress field in vicinity of seal and the interconnector groove interface. To achieve hermetic sealing the magnitude of stress in i) must create sufficient deformation to eliminate the gap and interconnection of micro channel network on the interfacial of the seal and groove surfaces. The collapse in micro channel on those surfaces at any particular loading would strongly related to ii) the stiffness and plastic behavior of the material being used at that temperature. Lastly, the interface where the stress value satisfies such condition must be large enough to ensure zero probability of gas to leak into those channels. An analysis is being carried out elsewhere to determine this relationship which will be adopted as a design criterion for compressive sealing technique.

4. Conclusions

The interconnector joint design for compressive seals based on a square, U and triangular groove have been investigated under SOFC operating condition. The stress distribution on cross section of the sealing material was calculated using finite element method (FEM). Conclusions are drawn from the present research as follows:

1. The obtained stress–strain curves of silver seal at different temperatures reveals that the tensile strength and elastic modulus decrease with increasing temperature. Small discrepancies are observed from the validation study using the profile curve of the seal's cross section.
2. The maximum stress is found at corner of the groove for square groove configuration, but the maximum stress for U and triangular grooves are highest at contacting surface between groove and material seal at the top location. The maximum stress of U groove is higher than that of the triangular and square grooves.
3. The extent of seal contact surface inside the square groove at the top location does not change with temperature. In contrast, for those in U and triangular grooves are small at ambient condition and increase with temperature because of softening effect.
4. U groove design is more robust than square and triangular groove designs, as it can maintain sufficiently high contact stress far exceeding the elastic limit over entire temperature range under this investigation resulting in lower leak rate.
5. The stress analysis suggests relatively greatest region of sufficiently high compressive stress for U-shape design whereas the triangular design posses lower stress with smaller region and the square design yields the lowest stress with greatest contact region.
6. The associated stress distribution suggests that the gasket has permanently deformed toward the U-shape wall surface at a greater degree than those for triangular shape design.
7. For U groove design, the leak rate is less than that of the triangular and square groove. The U-shape configuration

provides the best performance with immeasurable leak rate under the applying load of 0.67 MPa. The leak rate decreases with increasing pressure and temperature.

Currently, an investigation is being carried out to identify the relationship between the region of deformed gasket and the reduction in interconnectivity and the effective channel size of micro channel on the interface between the gasket and the interconnector surfaces.

Acknowledgment

The authors would like to thanks for financial support from Office of the Higher Education Commission, National Metal and Materials Technology Center, Energy Policy and Planning Office, Mahanakorn University of Technology and King Mongkut's Institute of Technology Ladkrabang.

References

[1] L.K.C. Tse, S. Wilkins, N. McGlashan, B. Urban, R. Martinez-Botas, J. Power Sources 196 (6) (2011) 3149–3162.
[2] S.H. Chan, H.K. Ho, Y. Tian, J. Hydrogen Energy 28 (8) (2003) 889–900.
[3] N. Punbusayakul, S. Charojrochkul, J. Charoensuk, B. Fungtammasan, Conf. Green and Sustainable Innovation 2 (2009) 125.
[4] J.W. Fergus, J. Power Sources 147 (2) (2005) 46–57.
[5] Y.-S. Chou, J.W. Stevenson, R.N. Gow, J. Power Sources 168 (2) (2007) 426–433.
[6] Y.-S. Chou, J.W. Stevenson, R.N. Gow, J. Power Sources 170 (2) (2007) 395–400.
[7] Y.-S. Chou, J.W. Stevenson, P. Singh, J. Power Sources 184 (1) (2008) 238–244.
[8] M.J. Pascual, A. Guillet, A. Duŕan, J. Power Sources 169 (1) (2007) 40–46.
[9] N. Punbusayakul, W. Wongklang, K. Wongtida, J. Charoensuk, S. Charojrochkul, J. Adv. Mater. Res. 55–57 (2008) 817–820.
[10] A. Jinnapat, S. Jiamsirilert, S. Charojrochkul, Proc. Adv. Technol. Mater. Mater. 9 (2007) 109–114.
[11] F. Smeacetto, M. Salvo, M. Ferraris, J. Cho, A.R. Boccaccini, J. Eur. Ceram. Soc. 28 (2008) 61–68.
[12] F. Smeacetto, M. Salvo, M. Ferraris, V. Casalegno, P. Asinari, J. Eur. Ceram. Soc. 28 (2008) 611–616.
[13] K.A. Nielsen, M. Solvang, S.B.L. Nielsen, A.R. Dinesen, D. Beeaff, P.H. Larsen, J. Eur. Ceram. Soc. 27 (2007) 1817–1822.
[14] Y.-S. Chou, J.W. Stevenson, L.A. Chick, J. Power Sources 112 (1) (2002) 130–136.
[15] Y.-S. Chou, J.W. Stevenson, J. Power Sources 112 (2) (2002) 376–383.
[16] M. Bram, S. Reckers, P. Drinovac, J. Mönch, R.W. Steinbrech, H.P. Buchkremer, D. Stöver, J. Power Sources 138 (1) (2005) 111–119.
[17] Y.-S. Chou, J.W. Stevenson, J. Mater. Res. 18 (2003) 2243–2250.
[18] Y.-S. Chou, J.W. Stevenson, J. Power Sources 191 (2) (2009) 384–389.
[19] B. Kuhn, F.J. Wetzel, J. Malzbender, R.W. Steinbrech, L. Singheiser, J. Power Sources 193 (1) (2009) 199–202.
[20] B. Kuhn, E. Wessel, J. Malzbender, R.W. Steinbrech, L. Singheiser, J. Power Sources 35 (17) (2010) 9158–9165.
[21] J. Duquette, J.W. Stevenson, J. Power Sources 137 (1) (2004) 71–75.
[22] K.S. Weil, C.A. Coyle, J.T. Darsell, G.G. Xia, J.S. Hardy, J. Power Sources 152 (1) (2005) 97–104.
[23] M.C. Tucker, C.P. Jacobson, L.C.D. Jonghe, S.J. Visco, J. Power Sources 160 (2) (2006) 1049–1057.
[24] A. Nakajo, Z. Wuillemin, J.V. Herle, D. Favrat, J. Power Sources 193 (1) (2009) 203–215.
[25] A. Nakajo, Z. Wuillemin, J.V. Herle, D. Favrat, J. Power Sources 193 (1) (2009) 216–226.
[26] C.-K. Lin, L.-H. Huang, L.-K. Chiang, Y.-P. Chyou, J. Power Sources 192 (2) (2009) 515–524.
[27] K.S. Weil, B.J. Koeppel, J. Hydrogen Energy 33 (14) (2008) 3976–3990.
[28] T.L. Jiang, M.-H. Chen, J. Hydrogen Energy 34 (19) (2009) 8223–8234.
[29] K. Boonsiri, N. Punbusayakul, S. Charojrochkul, J. Charoensuk, Conf. Energy Network of Thailand 7 (2011) 739–744.
[30] N. Punbusayakul, K. Boondiri, S. Charojrochkul, J. Charoensuk, Conf. Energy Network of Thailand 7 (2011) 994–998.
[31] N. Suksam, S. Charojrochkul, J. Charoensuk, Conf. Green and Sustainable Innovation 2 (2009) 120.
[32] G.R. Johnson, W.H. Cook, J. Eng. Fract. Mech. 21 (1) (1985) 31–48.
[33] C.-K. Lin, T.-T. Chen, Y.-P. Chyou, L.-K. Chiang, J. Power Sources 164 (1) (2007) 238–251.
[34] N. Punbusayakul, S. Charojrochkul and J. Charoensuk, Numerical modeling for prediction of thermo-mechanical properties of Aluminum for SOFC Operation, to be published.